Dalton Transactions

Accepted Manuscript

ROYAL SOCIETY OF CHEMISTRY

www.rsc.org/dalton

Dalton Transactions

Dynamic Article Links ►

Cite this: DOI: 10.1039/c4dt00000x

www.rsc.org/Dalton Trans.

ARTICLE

Structural Diversity and Magenetic Properties of Six Metal-Organic Polymers Based on Semirigid Tricarboxylate Ligand of 3,5-Bi(4-carboxyphenoxy)benzoic Acid

Liming Fan,[a,b] Weiliu Fan,[a] Weikuo Song,[b] Liming Sun,[a] Xian Zhao,*[a] Xiutang Zhang*[a,b]

Received (in XXX, XXX) Xth XXXXXXXXX 2014, Accepted Xth XXXXXXXXX 2014
DOI: 10.1039/c4dt00000x

ABSTRACT: Solvothermal reactions of the semirigid 3,5-bi(4-carboxyphenoxy)benzoic acid (H_3BCP) and transitional metal cations with the help of three ancillary bridging imidazole linkers afford six coordination polymers, namely, $[Co(HBCP)(1,4\text{-bib})_{0.5}]_n$ (**1**), $\{[Mn_{1.5}(BCP)(1,4\text{-bib})_{0.5}(\mu_2\text{-}H_2O)(H_2O)_2]\cdot(1,4\text{-bib})_{0.5}\}_n$ (**2**), $\{[Mn_{0.5}(1,4\text{-bib})(H_2O)]\cdot(H_2BCP)\}_n$ (**3**), $\{[Fe(BCP)_{0.5}(HCOO)_{0.5}(4,4'\text{-bibp})_{0.5}]\cdot 2H_2O\}_n$ (**4**), $[Ni_{2.5}(HBCP)(BCP)(4,4'\text{-bibp})_2(\mu_2\text{-}H_2O)(H_2O)_2]_n$ (**5**), and $[Ni(HBCP)(1,4\text{-bidb})_{1.5}(H_2O)_2]_n$ (**6**), (1,4-bib = 1,4-bis(1H-imidazol-4-yl)benzene, 1,4-bidb = 1,4-bis(1-imidazol-yl)-2,5-dimethyl benzene, 4,4'-bibp = 4,4'-bis(imidazol-1-yl)biphenyl). Their structures and properties have been determined by single-crystal and powder X-ray diffraction analyses, IR spectra, elemental analyses, thermogravimetric analyses (TGA), and X-ray photoelectron spectroscopy (XPS). Complex **1** displays an unusual 2D+2D→2D parallel entangled networks consisting of (3,4)-connected **3,4L83** sheets. Complex **2** exhibits an interesting 2-fold interpenetrated framework with the trinodal (4,4,6)-connected $(3\cdot4\cdot5\cdot6^2\cdot7)_2(3\cdot6\cdot7^4)_2(3^2\cdot4^2\cdot5^2\cdot6^2\cdot7^6\cdot9)$ topology. The host network of complex **3** is a 2D 4-connected $(4^4\cdot6^2)$-**sql** sheet. Complex **4** affords unprecedented 3D (4,6,6)-coordinated framework with point symbol of $(4^5\cdot6)(4^8\cdot6^7)(4^9\cdot6^3\cdot8^3)_2$, in which the 1D helix water chains occupy the void channels. Complex **5** can be regarded as a novel self-penetrating (4,4,4,5)-coordinated framework with point symbol of $(4\cdot5^4\cdot6)_2(4\cdot6^5\cdot7\cdot8^3)_2(5\cdot6\cdot7\cdot8^3)_2(5^2\cdot8^3\cdot9^2)$, which contains two interpenetrated (3,4,4,5)-coordinated $(4\cdot5^4\cdot6)_2(4\cdot6^5\cdot7\cdot8^3)_2(5\cdot6\cdot7)_2(5^2\cdot8^3\cdot9^2)$ subnets linked by μ_2-H_2O. Complex **6** shows a 1D ladder chain, which are further assembled into a 3D supramolecular structure *via* O−H···O and π···π interactions. Besides, magnetic studies indicate both complex **2** and **4** showing antiferromagnetic properties.

Introduction

The functional coordination polymers (CPs), as a class of novel solid materials, have been attracted thousands of coordination chemists and engineers for their intersting structures as well as potential applications in gas seperation and storage, catalysis, magnetsm, optical properties, and microelectronics sensing.[1-4] The architectures and functions of these materials can be tailored by altering the such factors as the metal cations, solvent media, templating agent, pH value, counteranion, and the chemical structure of organic ligands.[5-7] Strategically design or select featured organic ligand according to their length, rigidly, coordination modes, and functional groups or substituent was proved to be one efficient route for achieving expected CPs.[8]

Quite recently, semirigid multicarboxylate ligands with two or more aromatic rings separated by the nonmetallic atoms (C, N, O, Si, S atom) were employed to build interesting coordination frameworks, especially some flexible networks with breathing.[9] The flexibility of the organic semirigid multicarboxylate ligands endowed the constructed functional CPs tunable structures, which further have influence on the properties.[10] Owing to the valence electron configuration of those nonmetallic atoms, the semirigid linkers have a trend to coordinate inorganic nodes with characteristic shapes. Besides, when the ancillary ligands were introduce to bulid the networks, the final packing architectures have greater tunability.[11] Recent study shows that ancillary bridging imidazole linkers holding different lengths and flexibilities have great effects on the final packing supramolecular and topology as well as coordination modes and molecular conformations of host aromatic multicarboxylate acids.[12] As we all known, the mixed ligand strategy added the scope of the functional CPs, giving diversified polymeric structures with intersting structures and unusual properties. Therefore, it is worth trying to prepare novel functional metal-organic hybrid complexes by using such kind of semirigid multicarboxylate and ancillary bridging imidazole linkers.

[a] *State Key Laboratory of Crystal Materials, Shandong University , Jinan 250100, China. E-mail: zhaoxian@icm.sdu.edu.cn.*
[b] *Advanced Material Institute of Research, College of Chemistry and Chemical Engineering, Qilu Normal University, Jinan, 250013, China. E-mail: xiutangzhang@163.com.*

†Electronic Supplementary Information (ESI) available: Additional Figures, IR spectrum, Powder XRD patterns and X-ray crystallographic data, CCDC-986462 for **1**, 986460 for **2**, 986461 for **3**, 1006437 for **4**, 986464 for **5**, and 986463 for **6**. See DOI: 10.1039/c4dt00000x.

Thus, the aforementioned points inspired us to assembly novel coordination frameworks with semirigid 3,5-bi(4-carboxyphenoxy)benzoic acid (H_3BCP) and three ancillary bridging imidazole linkers (1,4-bib, 1,4-bidb, and 4,4'-bibp, Scheme 1). Herein, six novel CPs, with the structures ranged from 1D ladder chain (**6**), 2D sheet (**3**), 2D→2D parallel entangled network (**1**), 3D intriguing (4,6,6)-connected framework (**4**), 3D self-penetrating framework (**5**), to 3D→3D parallel entangled framework (**2**) (Scheme 2), were obtained through the mix ligand strategy under similar solvothermal reactions. Besides, magnetic studies indicate both complex **2** and **4** showing antiferromagnetic properties.

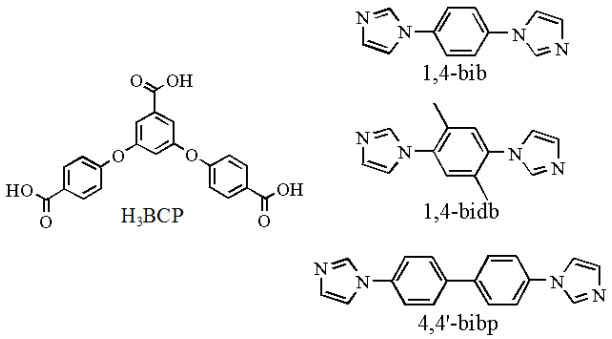

Scheme 1. Structures of H_3BCP and ancillary bridging imidazole linkers.

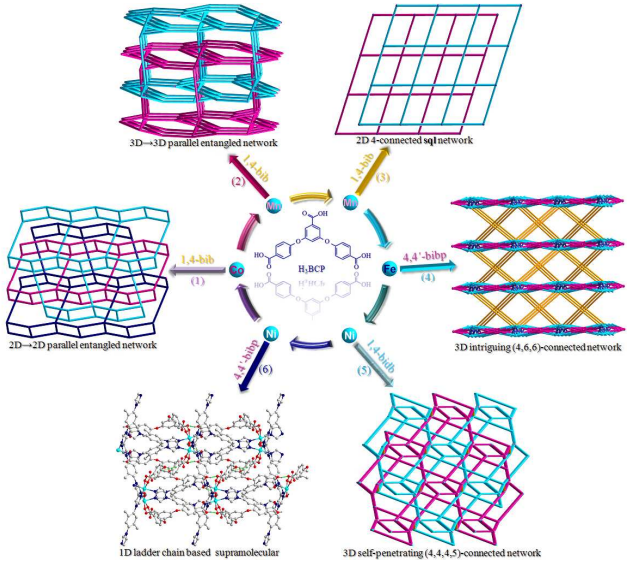

Scheme 2. Diversified polymeric structures of complexes **1**–**6.**

Experimental Section

Materials and Methods. All the chemical reagents were purchased from Jinan Henghua Sci. & Tec. Co. Ltd. without further purification. IR spectra were measured on a NEXUS 670 FTIR spectrometer. Elemental analyses were carried out on a CE instruments EA 1110 elemental analyzer. X-ray powder diffractions were measured on a Panalytical X-Pert pro diffractometer with Cu-Kα radiation. Thermogravimetric analyses (TGA) were performed under air condition on Perkin-Elmer TGA-7 thermogravimetric analyzer. The variable-temperature magnetic susceptibility measurements were performed on the Quantum Design SQUID MPMS XL-7 instruments. The XPS measurements were performed using a VG 220i XL system with 12.5 eV as pass energy and monochromatic Al*Ka* X-ray excitation.

General Synthesis and Characterization. All the titled compelxes are synthesised under simialr conditions with the mixture of H_3BCP, ancillary imidazole linkers (1,4-bib, 1,4-bidb, or 4,4'-bibp), and transitional metal salts added in H_2O or mixed sovlents. The NaOH was added to eliminate the protons of H_3BCP. After 170 °C heated for 3 days, the suitalbe crystals were obtained. Besides, the formate anion in complex **4** were believed derived from the decarboxylation of H_3BCP under high temperature and hgih pressure conditions.[13] To check the phase purity of **1**−**6**, PXRD has been introduced, the comparisons of measured and simulated PXRD patterns shows the main peaks are aligned with each other, which indicated the high purity of the complex (Fig. S1 and S2, see Supporting Information). For **1-6**, the IR absorption bands in the range of 3400-3500 cm^{-1} can be attributed to the characteristic peaks of O-H vibrations. The vibrations at ca. 1530 and 1620 cm^{-1} correspond to the asymmetric and symmetric stretching vibrations of the carboxyl groups, respectively (Fig. S3).

Synthesis of $[Co(HBCP)(1,4\text{-bib})_{0.5}]_n$ (1). A mixture of H_3BCP (0.15 mmol, 0.059 g), 1,4-bib (0.30 mmol, 0.063 g), $CoCl_2·6H_2O$ (0.30 mmol, 0.071 g), NaOH (0.40 mmol, 0.016 g) and 12 mL H_2O was placed in a Teflon-lined stainless steel vessel, heated to 170 °C for 3 days (After reaction, the pH=6.7), followed by slow cooling (a descent rate of 10 °C/h) to room temperature. Violet block crystals of **1** were obtained. Yield of 48% (based on Co). Anal. (%) calcd. for $C_{27}H_{17}CoN_2O_8$: C, 58.29; H, 3.08; N, 5.04. Found: C, 58.31; H, 3.11; N, 4.96. IR (KBr pellet, cm^{-1}): 3401 (w), 3126 (m), 1696 (w), 1577 (vs), 1529 (vs), 1376 (s), 1215 (s), 841 (m), 781 (m), 744(w).

Synthesis of $\{[Mn_{1.5}(BCP)(1,4\text{-bib})_{0.5}(\mu_2\text{-}H_2O)(H_2O)_2]·(1,4\text{-bib})_{0.5}\}_n$ (2). A mixture of H_3BCP (0.15 mmol, 0.059 g), 1,4-bib (0.30 mmol, 0.063 g), $MnSO_4·H_2O$ (0.30 mmol, 0.051 g), NaOH (0.40 mmol, 0.016 g) and 12 mL H_2O was placed in a Teflon-lined stainless steel vessel, heated to 170 °C for 3 days (After reaction, the pH=7.2), followed by slow cooling (a descent rate of 10 °C/h) to room temperature. Colourless block crystals of **2** were obtained. Yield of 53% (based on Mn). Anal. (%) calcd. for $C_{66}H_{52}Mn_3N_8O_{22}$: C, 53.63; H, 3.82; N, 7.58. Found: C, 53.51; H, 3.87; N, 7.76. IR (KBr pellet, cm^{-1}): 3114 (m), 1608 (w), 1530 (vs), 1490 (m), 1312 (m), 1300 (s), 1279 (m), 1068 (s), 1056 (s), 840 (m), 757 (m), 728 (m).

Synthesis of $\{[Mn_{0.5}(1,4\text{-bib})(H_2O)]·(H_2BCP)\}_n$ (3). A mixture of H_3BCP (0.20 mmol, 0.079 g), 1,4-bib (0.30 mmol, 0.063 g), $MnSO_4·H_2O$ (0.30 mmol, 0.051 g), NaOH (0.10 mmol, 0.004 g), 9 mL H_2O, and 3 mL EtOH was placed in a Teflon-lined stainless steel vessel, heated to 170 °C for 3 days (After reaction, the pH=6.1), followed by slow cooling (a descent rate of 10 °C/h) to room temperature. Colorless block crystals of **3** were obtained. Yield of 68% (based on Mn). Anal. (%) calcd. for $C_{66}H_{50}MnN_8O_{18}$: C, 61.07; H, 3.88; N, 8.63. Found: C, 60.92; H, 3.90; N, 8.74. IR (KBr pellet, cm^{-1}): 3109 (m), 1689 (vs), 1587 (s), 1505 (m), 1471 (w), 1417 (s), 1287 (m), 1217 (s), 1167 (m), 857 (m), 771 (m)

Synthesis of $\{[Fe(BCP)_{0.5}(HCOO)_{0.5}(4,4'\text{-bibp})_{0.5}]·2H_2O\}_n$ (4). A mixture of H_3BCP (0.20 mmol, 0.079

Table 1 Crystal data for **1 – 6**.

Compound	**1**	**2**	**3**	**4**	**5**	**6**
Empirical formula	$C_{27}H_{17}CoN_2O_8$	$C_{66}H_{54}Mn_3N_8O_{22}$	$C_{66}H_{50}MnN_8O_{18}$	$C_{20}H_{13}FeN_2O_6$	$C_{156}H_{114}N_{16}Ni_5O_{38}$	$C_{42}H_{37}N_6NiO_{10}$
Formula weight	556.36	1475.99	1298.08	433.17	3114.18	844.49
Crystal system	Monoclinic	Monoclinic	Triclinic	Orthorhombic	Triclinic	Monoclinic
Space group	$P2_1/c$	$P2_1/n$	P-1	$Pcca$	P-1	$P2_1/c$
a (Å)	11.445(3)	16.899(3)	9.3105(9)	9.021(5)	14.5871(9)	13.964(4)
b (Å)	18.689(5)	11.245(2)	13.2138(13)	13.841(8)	16.6281(11)	19.227(3)
c (Å)	11.538(3)	18.736(4)	14.0990(14)	30.183(18)	17.3904(11)	14.812(6)
α (°)	90.00	90.00	102.310(2)	90.00	63.1710(10)	90.00
β (°)	111.085(4)	115.504(3)	108.444(2)	90.00	65.8790(10)	104.10(2)
γ (°)	90.00	90.00	108.378(2)	90.00	86.1310(10)	90.00
V(Å^3)	2302.7(12)	3213.4(10)	1464.1(2)	3769(4)	3399.8(4)	3856.9(7)
Z	4	2	1	8	1	4
D_{calcd} (Mg/m^3)	1.605	1.525	1.472	1.527	1.521	1.454
μ(mm^{-1})	0.804	0.667	0.311	0.841	0.773	0.572
θ range (°)	1.91–25.00	2.15–25.00	1.73–25.00	2.00–25.00	1.61–25.00	1.77–25.00
Reflections collected	11774	16066	7634	17974	17385	19784
Unique reflection	4053	5659	5129	3328	11646	6786
Data/Parameters	4053/344	5659/457	5129/431	3328/259	11646/983	6786/550
F(000)	1136	1514	671	1768	1606	1756
T(K)	296(2)	296(2)	293(2)	296(2)	296(2)	293(2)
R_{int}	0.0196	0.0294	0.0167	0.0378	0.0223	0.0346
R_1 (wR_2) [$I > 2\sigma(I)$]	0.0282 (0.0802)	0.0489 (0.1392)	0.0383 (0.1043)	0.0439 (0.1328)	0.0754 (0.1816)	0.0401 (0.1109)
R_1 (wR_2) (all data)	0.0342 (0.0848)	0.0617 (0.1528)	0.0439 (0.1094)	0.0542 (0.1435)	0.1050 (0.2080)	0.0539 (0.1179)
Gof	0.999	0.998	1.002	0.998	1.003	0.999

$R_1 = \Sigma||F_o|-|F_c|| / \Sigma|F_o|$, $wR_2 = [\Sigma w(F_o^2-F_c^2)^2] / \Sigma w(F_o^2)^2]^{1/2}$

g), 4,4'-bibp (0.30 mmol, 0.086 g), $FeSO_4 \cdot 7H_2O$ (0.20 mmol, 0.056 g), NaOH (0.20 mmol, 0.008 g) and 12 mL H_2O was placed in a Teflon-lined stainless steel vessel, heated to 170 °C for 3 days (After reaction, the pH=6.4), followed by slow cooling (a descent rate of 10 °C/h) to room temperature. Black green block crystals of **4** were obtained. Yield of 43% (based on Fe). Anal. (%) calcd. for $C_{20}H_{15}FeN_2O_6$: C, 55.20; H, 3.47; N, 6.43. Found: C, 54.83; H, 3.67; N, 6.302. IR (KBr pellet, cm^{-1}): 3119 (m), 1595 (s), 1515 (vs), 1398 (s), 1307 (s), 1277 (m), 1060 (s), 878 (w), 783 (m), 749 (w).

Synthesis of $[Ni_{2.5}(HBCP)(BCP)(4,4'\text{-bibp})_2(\mu_2\text{-}H_2O)(H_2O)_2]_n$ (5). A mixture of H_3BCP (0.20 mmol, 0.079 g), 4,4'-bibp (0.30 mmol, 0.086 g), $NiSO_4 \cdot 6H_2O$ (0.30 mmol, 0.079 g), NaOH (0.20 mmol, 0.008 g) and 12 mL H_2O was placed in a Teflon-lined stainless steel vessel, heated to 170 °C for 3 days (After reaction, the pH=6.4), followed by slow cooling (a descent rate of 10 °C/h) to room temperature. Green block crystals of **5** were obtained. Yield of 81% (based on Ni). Anal. (%) calcd. for $C_{156}H_{114}N_{16}Ni_5O_{38}$: C, 60.17; H, 3.69; N, 7.20. Found: C, 60.68; H, 3.71; N, 10.18. IR (KBr pellet, cm^{-1}): 3188 (m), 3061 (w), 1711 (m), 1560 (s), 1520 (vs), 1398 (vs), 1220 (s), 816 (m), 784 (m), 744 (w).

Synthesis of $[Ni(HBCP)(1,4\text{-bidb})_{1.5}(H_2O)_2]_n$ (6). A mixture of H_3BCP (0.20 mmol, 0.079 g), 1,4-bidb (0.20 mmol, 0.048 g), $NiSO_4 \cdot 6H_2O$ (0.40 mmol, 0.105 g), NaOH (0.30 mmol, 0.012 g) and 12 mL H_2O, and 2 mL DMF was placed in a Teflon-lined stainless steel vessel, heated to 170 °C for 3 days (After reaction, the pH=6.6), followed by slow cooling (a descent rate of 10 °C/h) to room temperature. Green block crystals of **6** were obtained. Yield of 56% (based on Ni). Anal. (%) calcd. for $C_{42}H_{37}N_6NiO_{10}$: C, 59.74; H, 4.42; N, 9.95. Found: C, 60.13; H, 4.28; N, 9.31. IR (KBr pellet, cm^{-1}): 3317 (s), 3139 (s), 1668 (m), 1595 (vs), 1317 (vs), 1381 (s), 1069 (s), 830 (m), 753 (m), 707 (w).

X-ray Crystallography. The crystal data was collected with a Siemens SMART diffractometer using Mo-Kα radiation (λ=0.71073Å) at room temperature. The structures of those titled complexes were solved by direct methods, with the non-hydrogen atoms refined anisotropically by using the SHELXTL package with F^2 values based full-matrix least-squares procedure.[14] All the hydrogen atoms except those for water molecules were generated geometrically with fixed isotropic thermal parameters, and included in the structure factor calculations. For **1**–**6**, crystallographic data and the selected bond lengths and angles are given in Table 1 and Table S1. Further details of crystal structure can be obtained from the Cambridge Crystallographic Data Centre, CCDC, 12 Union Road, CAMBRIDGE CB2 1EZ, UK, [Telephone: +44-(0)1223-762-910, Fax: +44-(0)1223-336-033; E-mail: deposit@ccdc.cam.ac.uk, http://www.ccdc.cam.ac.uk/deposit], on quoting the depository number CCDC-986462 for **1**, 986460 for **2**, 986461 for **3**, 1006437 for **4**, 986464 for **5**, and 986463 for **6**. Topological analysis was performed by using TOPOS program.[15]

Result and Discussion

Structural Description of $[Co(HBCP)(1,4\text{-bib})_{0.5}]_n$ (1). Structure analysis reveals complex **1** crystallizes in the monoclinic system, space group $P2_1/c$. The asymmetric unit consists of one Co^{II} ion, one $HBCP^{2-}$ ligand, and a half of 1,4-bib ligand (Fig. 1a). Each Co^{II} center is tetra-coordinated by three oxygen atoms from three different $HBCP^{2-}$ linkers [Co(1)–O(1) = 1.969(5), Co(1)–O(5) = 1.983(7), and Co(1)–O(7) = 1.983(0) Å], and one nitrogen atom from 1,4-bib ligand [Co(1)–N(1) = 1.992(4) Å]. The H_3BCP ligand is partially deprotonated and twisted with the dihedral angle between three phenyl rings are 71.7(5), 87.4(0), and 42.4(7)°, respectively. The three carboxyl groups coordinated with three Co^{II} ions with μ_1-η^1:η^0 coordination modes (Mode I, Scheme 3), leaving a 1D $[Co(HBCP)]_n$ ladder chain with the Co···Co distance is 10.696(7) Å (Fig. 1b). Then 1,4-bib ligand linked the 1D ladder chains,

forming an interestingly 2D sheet with the 60-membered large macrocycle (13.454(5)×18.659(5) Å^2) (Fig. 1c).

Each sheet can be defined as a (3,4)-connected $(4^2.6^3.8)(4^2.6)$-**3,4L83** layer with the Co^{II} ion and $HBCP^{2-}$ ligand regarded as four and three nodes, respectively. The large macrocycle within each sheet and the 1D $[Co(HBCP)]_n$ ladder chain make the neighbouring layers possible to interpenetrate with each other. Each sheet simultaneously penetrated with two another adjacent ones, finally formed a rarely reported 3-fold 2D→2D parallel entangled network (Fig. 1d).

Structural Description of $\{[Mn_{1.5}(BCP)(1,4\text{-bib})_{0.5}(\mu_2\text{-}H_2O)(H_2O)_2]\cdot(1,4\text{-bib})_{0.5}\}_n$ (2). When using Mn^{II} instead of the Co^{II} as centre metal ions, complex **2** with unusual 2-fold 3D→3D polycatenation was obtained. X-ray analysis reveals complex **2** crystallized in monoclinic system $P2_1/n$. As depicted in Fig. 2a, complex **2** consists of one and a half crystallographically independent Mn^{II} ions, one BCP^{3-} ligand, three coordinated water molecules, and half of 1,4-bib ligands. Mn(1) is hexa-coordinated by one N atom from 1,4-bib ligand, five O atoms from two different BCP^{3-} ligands, two mono-coordinated water molecules, and one bridging μ_2-H_2O, forming an octahedral coordination geometry with slightly distorted. Mn(2) is located in a distorted $[MnO_6]$ octahedral environment, completed by four carboxyl O atoms from four BCP^{3-} ligands and two O from μ_2-H_2O. The Mn−N distance is 2.178(3) Å, and the Mn−O lengths are 2.106(2)–2.268(2) Å.

The H_3BCP ligand in complex **2** is completely deprotonated and coordinates with four Mn^{II} ions by using two μ_1-η^1:η^0 carboxyl groups and one μ_2-η^1:η^1 carboxyl group (Mode II, Scheme 3). The dihedral angle between two side phenyl rings and central phenyl ring in BCP^{3-} are 54.2(1) and 80.7(0)°, respectively. And the one between two side phenyl rings is 58.8(5)°. It is worthy to note that three Mn^{II} ions are linking into one trinuclear $[Mn_3(COO)_6]$ cluster by sharing six μ_2-η^2:η^1 carboxyl groups, with the Mn···Mn distance is 3.830(9) Å. And the trinuclear SBUs are further expanded to a 2D $[Mn_3(BCP)_2]_n$ sheet (Fig. 2b). The 1,4-bib bridging linker act as pillars to support the 2D sheets, finally resulting in a 3D network (Fig. 2c). It is noteworthy that the guest molecules (1,4-bib, H_2O) occupied the channels *via* hydrogen bonds, which may be one important factor to stabilize the whole framework.

Topology analysis shows the whole network of complex **2** can be rationalized to a 2-fold 3D→3D interpenetrated (4,4,6)-connected networks with the point symbol of $(3\cdot4\cdot5\cdot6^2\cdot7)_2(3\cdot6\cdot7^4)_2(3^2\cdot4^2\cdot5^2\cdot6^2\cdot7^6\cdot9)$ topology by denoting both Mn ions as 4-connected nodes, the BCP^{3-} ligand as 6-connected nodes, respectively (Fig. 2d).

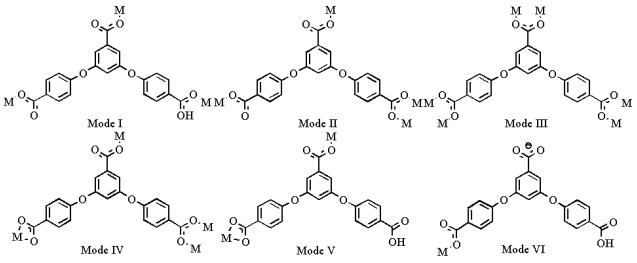

Scheme 3. The coordination modes of H_3BCP in complexes **1**–**6.**

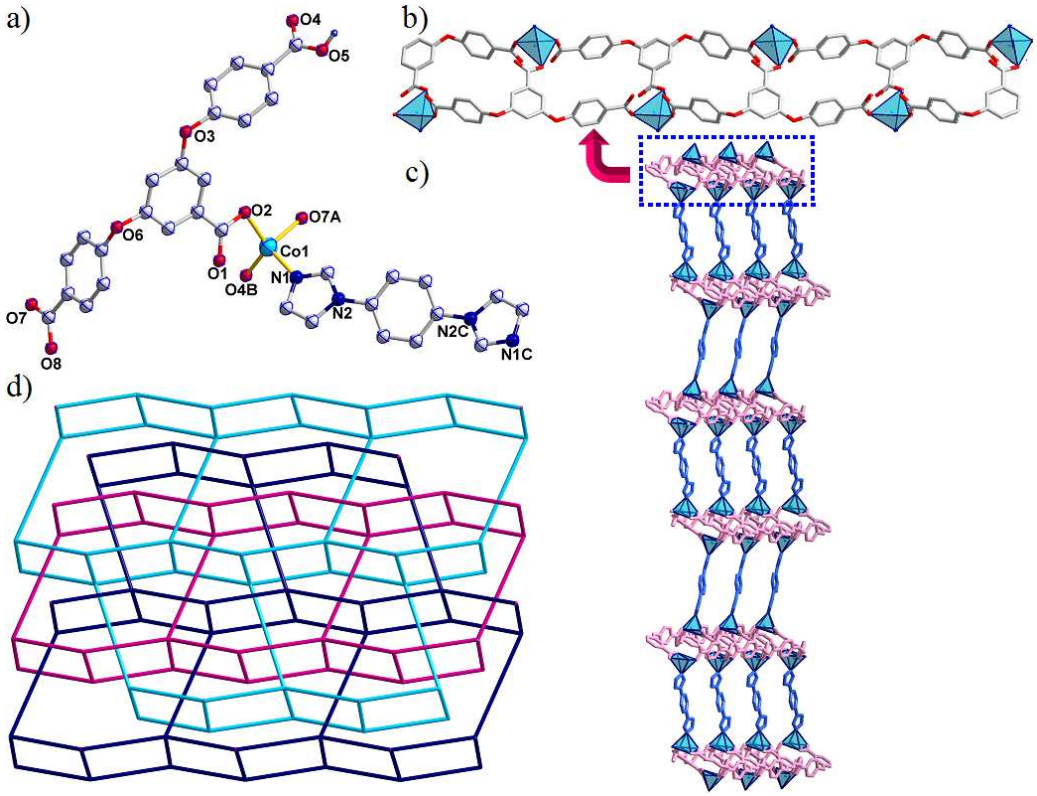

Figure 1. (a) The asymmetric unit of **1** (Symmetry codes: A: 1-*x*, -0.5+*y*, 0.5-*z*; B: 1-*x*, 0.5+*y*, 0.5-*z*; C: 1–*x*, 1-*y*, 2-*z*). (b) The 1D $[Co(HBCP)]_n$ ladder chain. (c) View of the 2D $[Co(HBCP)(1,4\text{-bib})_{0.5}]_n$ sheet constructed from the 1,4-bib bridged 1D ladder chains. (d) Schematic view of the 2D→2D (3,4)-connected **3,4L83** net with the Point Schläfli symbol of $(4^2.6^3.8)(4^2.6)$ in **1**.

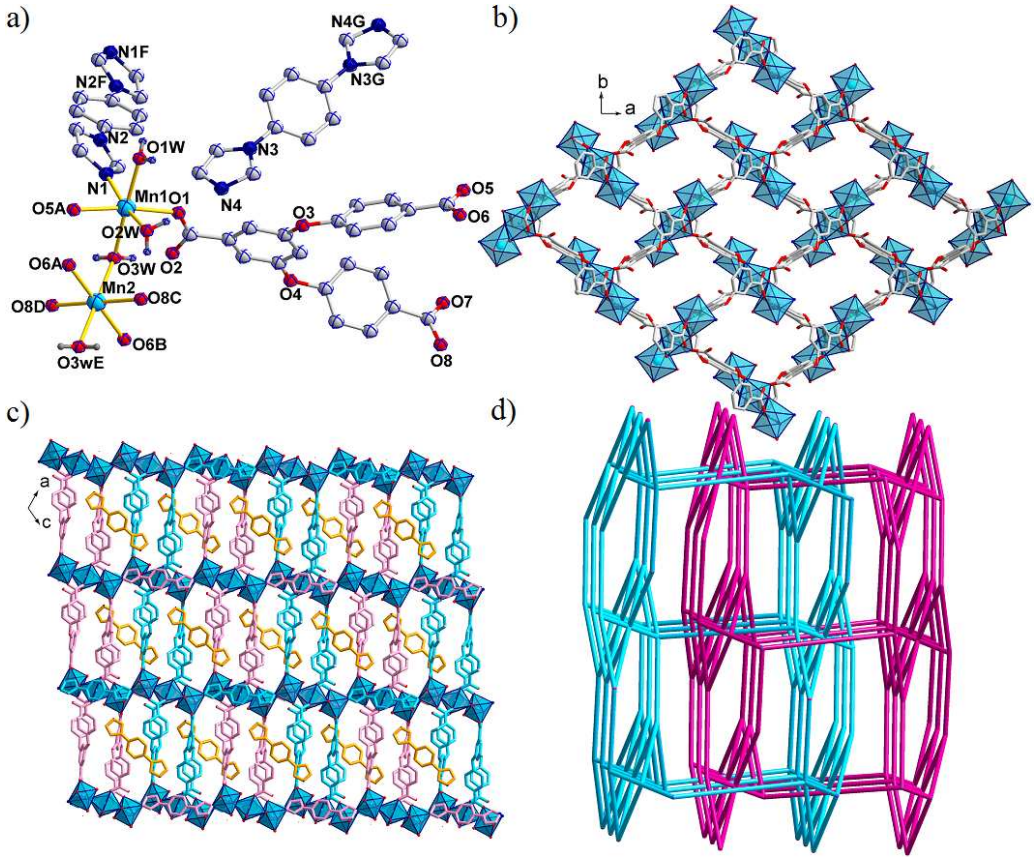

Figure 2. (a) The asymmetric unit of **2** (Symmetry codes: A: 0.5+*x*, 1.5-*y*, -0.5+*z*; B: 0.5-*x*, -0.5+*y*, 0.5-*z*; C: 0.5-*x*, 0.5+*y*, 0.5-*z*; D: 0.5+*x*, 0.5-*y*, -0.5+*z*; E: 1-*x*, 1-*y*, -*z*; F: 2-*x*, 1-*y*, 1-*z*; G: 1-*x*, 2-*y*, 1-*z*.). (b) The $[Mn_3(COO)_6]$ cluster based 2D $[Mn_3(BCP)_2]_n$ sheet view along *c* axis. (c) The 3D→3D parallel entangled networks view along *b* axis. (d) The 2-fold 3D→3D (4,4,6)-connected $(3\cdot4\cdot5\cdot6^2\cdot7)_2(3\cdot6\cdot7^4)_2(3^2\cdot4^2\cdot5^2\cdot6^2\cdot7^6\cdot9)$ topology in **2**.

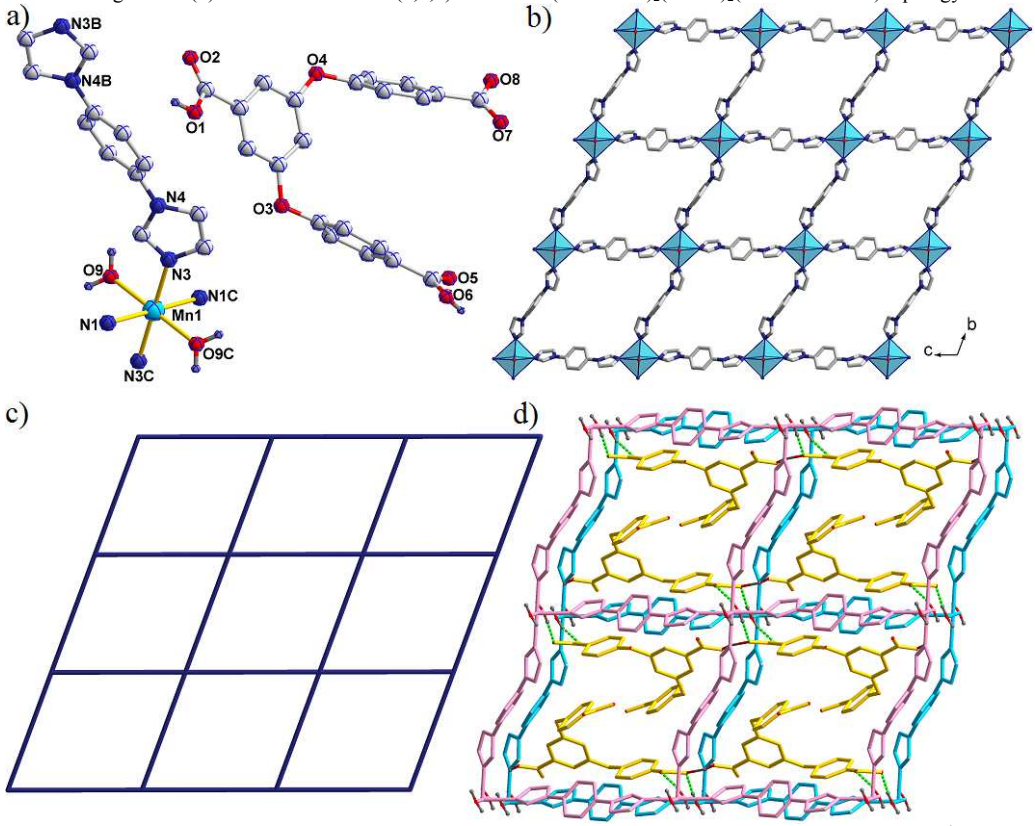

Figure 3. (a) The asymmetric unit of **3** (Symmetry codes: B: 2-*x*, 1-*y*, 1-*z*; C: 1-*x*, -*y*, 1-*z*). (b) The 4-connetced $[Mn(1,4\text{-bib})_2]_n^{2n+}$ networks. (c) The 2D 4-connetced $(4^4\cdot6^2)$-**sql** topology. (d) The 3D supramolecular of complex **3** connected though O-H···O hydrogen bonds.

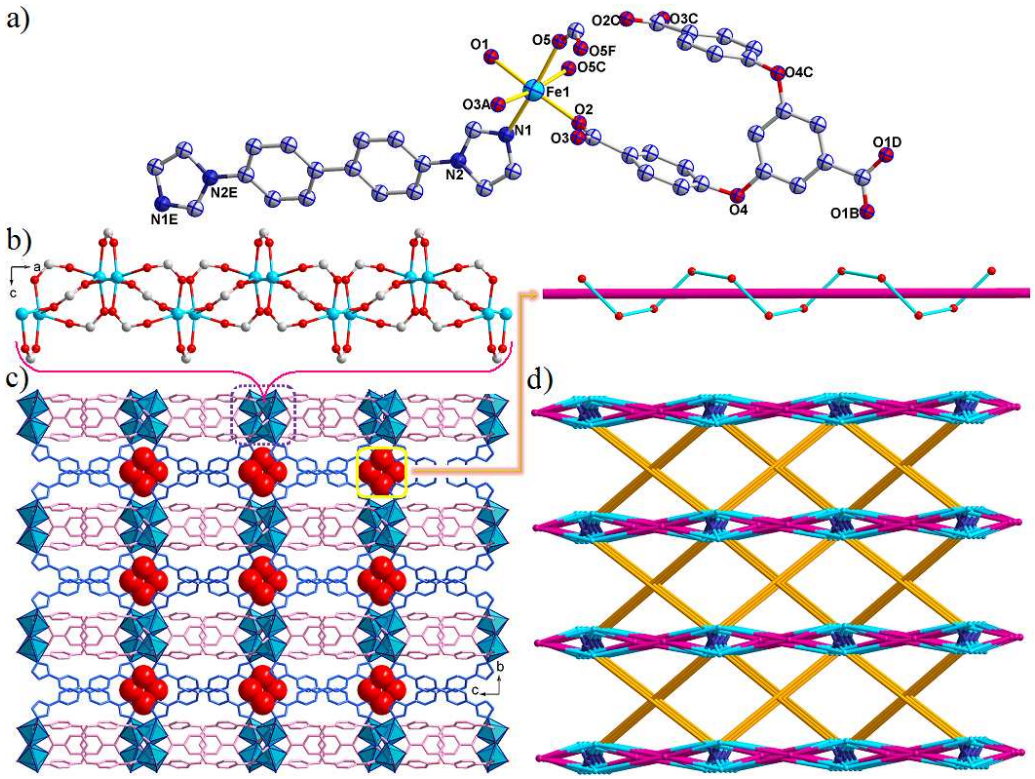

Figure 4. (a) The asymmetric unit of **4** (Symmetry codes: A: -*x*, *y*, 0.5-*z*; B: 0.5-*x*, *y*, -0.5+*z*; C: 0.5-*x*, 1-*y*, *z*; D: *x*, 1-*y*, -0.5+*z*; E: 1-*x*, 2-*y*, 1-*z*; F: -*x*, *y*, 0.5-*z*.). (b) The unprecedented 1D $[Fe_4(COO)_6(HCOO)_2]_n$ chain. (c) View of the 3D frameworks in which the 1D helix water chains occupied the void channels. (d) Schematic view of the novel (4,6,6)-coordinated framework with Point Schläfli symbol of $(4^5\cdot6)(4^8\cdot6^7)(4^9\cdot6^3\cdot8^3)_2$.

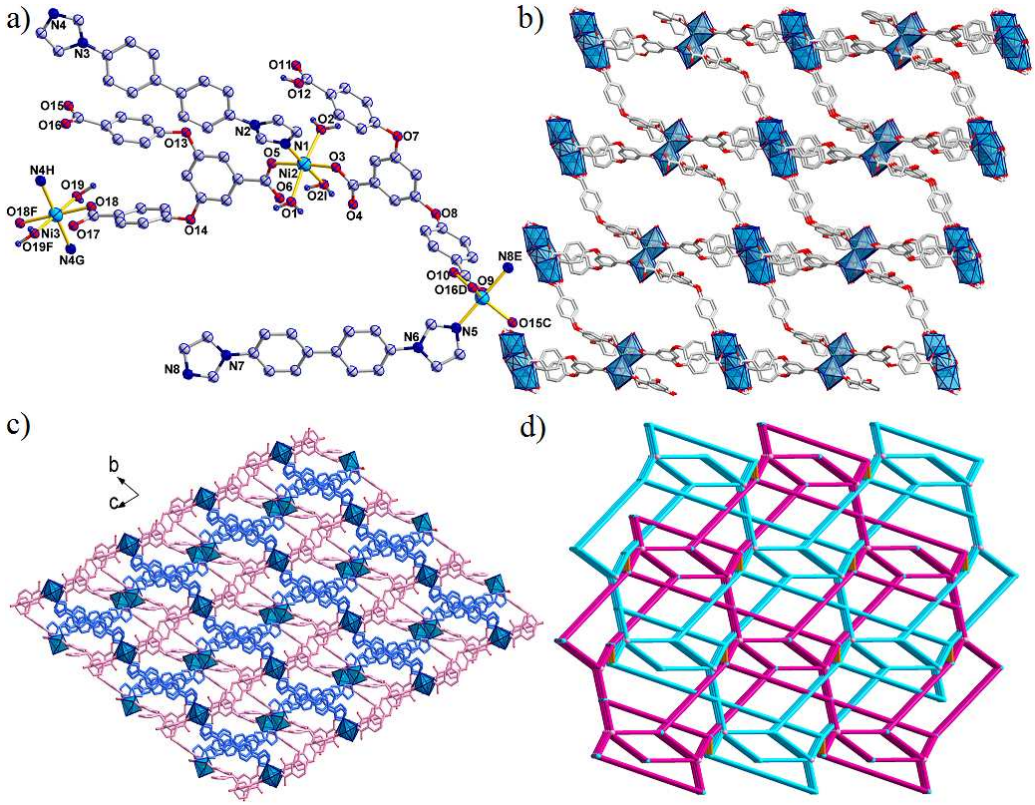

Figure 5. (a) The asymmetric unit of **5** (Symmetry codes: C: 1+*x*, -1+*y*, -1+*z*; D: 2-*x*, 1-*y*, 1-*z*; E: *x*, *y*, -1+*z*; F: -*x*, 1-*y*, 3-*z*; G: -1+*x*, -1+*y*, 1+*z*; H: 1-*x*, 2-*y*, 2-*z*.). (b) The 3D $[Ni_{2.5}(HBCP)(BCP)]_n$ network. (c) View of the 3D network along *bc* plane. (d) Schematic view of the novel self-penetrating (4,4,4,5)-coordinated network with Point Schläfli symbol of $(4\cdot5^4\cdot6)_2(4\cdot6^5\cdot7\cdot8^3)_2(5\cdot6\cdot7\cdot8^3)_2(5^2\cdot8^3\cdot9^2)$, which contains two interpenetrated (3,4,4,5)-coordinated $(4\cdot5^4\cdot6)_2(4\cdot6^5\cdot7\cdot8^3)_2(5\cdot6\cdot7)_2(5^2\cdot8^3\cdot9^2)$ subnets linked by μ_2-H_2O.

Structural Description of {[$Mn_{0.5}$(1,4-bib)(H_2O)]·(H_2BCP)}$_n$ (3). Similar reaction environment to **2**, except for the H_2O was replaced by H_2O/EtOH system, the 3D→3D parallel entangled network degrade to a 2D **sql** sheet. Complex **3** crystallizes in triclinic space group *P*-1. The asymmetric unit contains a half of crystallographically independent Mn^{II} ions, one 1,4-bib ligand, one protonated H_2BCP^- ion, and one lattice water (Fig. 3a). Crystal structure analysis shows that the Mn^{II} center is located in a hexa-coordinated slightly distorted octahedron, surrounded by four nitrogen atoms from four 1,4-bib ligands and two O_{water}. The Mn−N distances are 2.133(3)/2.211(7) Å, and Mn−O bond length is 2.088(9) Å.

The H_3BCP ligands in complex **3** are partly deprotonated and act as anions, instead of participating in coordination to metal ions. Mn^{II} ions are connected by 1,4-bib ligands resulting in a 4-connected 2D $[Mn(1,4\text{-bib})_2]_n^{2n+}$ layer with the opening area is about 13.554(1)×14.099(0) $Å^2$, exhibiting a $(4^4\cdot6^2)$-**sql** topology (Fig. 3b and 3c). Furthermore, with the help of O-H···O [O1−H1···O8^i = 2.472(1) Å, O9^{ii}-H2w^{ii}···O7 = 2.780(6) Å O9^{iii}-H1w^{iii}···O8 = 2.740(4) Å, Symmetry codes: i: *x*, *y*, -1+*z*; ii: *x*, *y*, -1+*z*; iii: *x*, *y*, -1+*z*.], finally given a stable 3D supramolecular architecture (Fig. 3d).

Structure descriptions of {[Fe(BCP)$_{0.5}$(HCOO)$_{0.5}$(4,4'-bibp)$_{0.5}$]·2H_2O}$_n$ (4). Complex **4** crystallizes in the orthorhombic crystal system *P*cca. As shown in Fig. 4a, each Fe^{II} ion is hexa-coordinated, completed by five oxygen atoms from three different BCP^{3-} ligands and two $HCOO^-$ anions, and one nitrogen atoms from the 4,4'-bibp ligand, leaving a distorted octahedral coordination geometry. The bond lengths of Fe–O are in the range of 2.052(2)–2.290(2) Å, and the Fe–N bond distance is 2.180(3) Å.

In complex **4**, each carboxyl group of BCP^{3-} ligand exhibits bridging μ_2-η^1:η^1 coordination mode (Mode III). And $HCOO^-$ anion adopts μ_4-η^2:η^2 bridging coordination mode. Fe^{II} cations are bridged by μ_2-η^1:η^1 carboxyl groups and μ_4-η^2:η^2- $HCOO^-$ anions to generate 2D layer, including 1D $[Fe_4(COO)_6(HCOO)_2]_n$ chains with the Fe···Fe distances being 3.399(8) Å, 4.089(5) Å, and 5.921(2) Å (Fig. 4b). Then the adjacent 2D layers are bridged by 4,4'-bibp linkers to form a 3D framework (Fig. 4c). It is noteworthy that the solvent water molecules interacted with each other through O−H···O hydrogen bonds (d(D···A)=3.163(3) Å,∠(D−H···A) = 128.9(8)º), forming an interestingly 1D helix water chain.

From the viewpoint of structural topology, the final packing structure exhibits a (4,6,6)-connected framework with Point Schläfli symbol of $(4^5\cdot6)(4^8\cdot6^7)(4^9\cdot6^3\cdot8^3)_2$ by denoting Fe^{II} cations and BCP^{3-} ligands as 6-connected nodes, $HCOO^-$ anion as 4-connected nodes (Fig. 4d).

Structure descriptions of [$Ni_{2.5}$(HBCP)(BCP)(4,4'-bibp)$_2$(μ_2-H_2O)(H_2O)$_2$]$_n$ (5). Structure analysis reveals complex **5** is an unprecedented self-pentetraing net, which has never been reported before. Complex **5** contains two and a half of Ni^{II} ions, one completely deprotonated BCP^{3-} ligand, one partly deprotonated $HBCP^{2-}$ ligand, two 4,4'-bibp bridging linkers, one μ_2-H_2O, and two mono-coordinated water molecules. Shown in Fig. 6a, Ni(1) is hexa-coordinated by two N atom from two 4,4'-bibp bridging linkers and four oxygen atoms from two BCP^{3-} ligands and one $HBCP^{2-}$ ligand, resulting in a distorted octahedral coordination geometry. While the coordination environment of Ni(2) located in a centrosymmetric NiO_4N_2 octahedral geometry, completed by two O atoms from BCP^{3-} ligands and two water molecules, and two N atoms from two 4,4'-bibp ligands. Ni(3) exhibiting similar coordination geometry, hexa-coordinated by two N atoms from the imidazole of 4,4'-bibp linkers, and four O atoms from two BCP^{3-} ligand and two water molecules. The Ni-N and Ni−O bond lengths are in the range of 2.058(5)−2.070(6) Å and 2.012(5)−2.112(8) Å, respectively.

The ligand of BCP^{3-} acts as one μ_4 node to coordinate with four Ni^{II} ions, in which three carboxyl groups adopt μ_1-η^1:η^0, μ_1-η^1:η^1, and μ_2-η^1:η^1 coordination mode, respectively (Mode IV, Scheme 3), with the dihedral angles among the three phenyl rings being 86.5(6), 85.6(3), and 18.1(8)°, respectively. While the partly deprotonated $HBCP^{2-}$ acts as bridging linker to link with two Ni^{II}, with the two deprotonated carboxyl groups adopt μ_1-η^1:η^0 and μ_1-η^1:η^1 coordination mode, respectively (Mode V, Scheme 3), and the dihedral angles in $HBCP^{2-}$ are 71.0(9), 76.7(2), and 11.3(7)°, respectively. Ni^{II} ions are linked by BCP^{3-} and $HBCP^{2-}$ ligands, successfully constructed a 2D layer, which was further expanded by μ_2-H_2O to give a 3D $[Ni_{2.5}(HBCP)(BCP)(\mu_2\text{-}H_2O)]_n$ network (Fig. 5b). Interestingly, the linear 4,4'-bibp linkers which act as pillars to coordinate Ni^{II} ions of the layers, as well as the monodentate 4,4'-bibp ligands, both contribute to the stable of final structure (Fig. 5c).

From the viewpoint of topology, the final obtained 3D structure exhibits as an interestingly tetranodal (4,4,4,5)-connected 3D frameworks with the Point Schläfli symbol of $(4\cdot5^4\cdot6)_2(4\cdot6^5\cdot7\cdot8^3)_2(5\cdot6\cdot7\cdot8^3)_2(5^2\cdot8^3\cdot9^2)$ by denoting Ni(1), Ni(2), Ni(3), BCP^{3-} as 5-connected, 4-connected, 4-connected, 4-connected nodes, respectively (Fig. 5d). It is worth noting that the whole structure can be seen as a self-pentetraing nets, because the final structure can be easily simplified to a 2-fold interpenetrated (3,4,4,5)-connected $(4\cdot5^4\cdot6)_2(4\cdot6^5\cdot7\cdot8^3)_2(5\cdot6\cdot7)_2(5^2\cdot8^3\cdot9^2)$ subnets by omitting μ_2-H_2O-Ni bonds. To the best of our knowledge, the topologies of both the sbunets and frameworks have never been documented up to now.

Structural Description of [Ni(HBCP)(1,4-bidb)$_{1.5}$(H_2O)$_2$]$_n$ (6). When the long 4,4'-bibp ancillary bridging linker was replaced by the methyl group modified shorting ligand, the steric effects and supporting requirements of neighbouring ions make another trendy. Structure analysis reveals complex **6** is a 1D ladder chains, rather than 2D layers or 3D nets. Complex **6** crystallizes in monoclinic crystal system $P2_1/c$. As can be seen in Fig. 6a, the asymmetric unit contained one crystallographically independent Ni^{II} ion, one partly deprotonated $HBCP^{2-}$ ligand, one and a half of 1,4-bidb, and two coordinated water molecules. Each Ni^{II} canter is located in a distorted $[NiN_3O_3]$ octahedral geometry, completed by three O atoms from one $HBCP^{2-}$ ligand and two coordinated water molecules, three nitrogen atoms from different 1,4-bidb bridging ligands.

The Ni^{II} ions are bridged by 1,4-bidb ligands to generate an infinite 1D $[Ni(1,4\text{-bidb})]_n$ ladder structure (Fig. 6b), with the 1,4-bidb separated Ni···Ni distance is 2.778(3) Å. With the help of O−H···O hydrogen bonds (O5···H5A−O3=2.438(3) Å, O1w···H1w−O6=2.686(3) Å, and O2w···H3w−O2=2.778(3) Å.)

and π···π interactions ((D···A)=3.833(7) Å) between adjacent chains, the final 3D supramolecular structure was formed (Fig.6c).

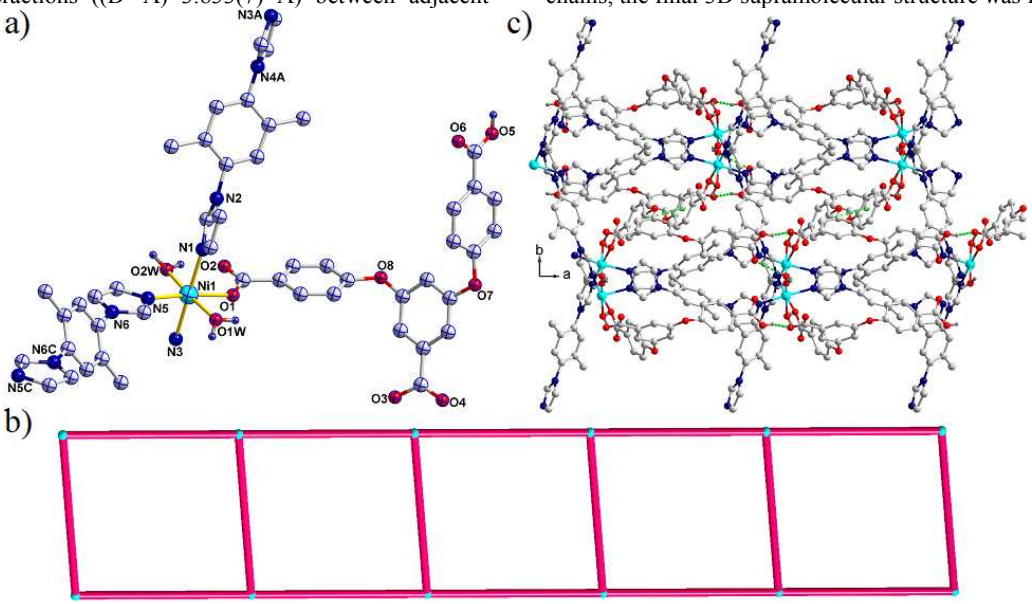

Figure 6. (a) The asymmetric unit of **6** (Symmetry codes: A: 1–*x*, *y*, 1.5-*z*; B: *x*, 1-*y*, 0.5+*z*; C: 1-*x*, 1-*y*, 1-*z*). (b) The simplified 1D ladder chain of complex **6**. (c) The 3D supramolecular of complex **6**.

Table 2 The detailed comparisons of complexes **1**–**6**.

Complex	Coord. Modes	Ancillary Linkers/Role	Dihedral Angles (°)	Structure and Topology
1	Mode I	1,4-bib/bridging	87.4(0)/42.4(7)/71.7(5)	2D→2D (3,4)-connected parallel entangled $(4^2.6^3.8)(4^2.6)$-**3,4L83** net
2	Mode II	1,4-bib/bridging+guest	54.7(7)/80.7(8)/58.4(9)	3D→3D (4,4,6)-connected $(3\cdot4\cdot5\cdot6^2\cdot7)_2(3\cdot6\cdot7^4)_2(3^2\cdot4^2\cdot5^2\cdot6^2\cdot7^6\cdot9)$ net
3	N/A	1,4-bib/bridging	73.8(5)/68.8(0)/23.0(8)	2D 4-connected $(4^4\cdot6^2)$-**sql** sheet
4	Mode III	4,4'-bibp/bridging	88.7(5)/88.7(5)/9.9(4)	3D (4,6,6)-coordinated $(4^5\cdot6)(4^8\cdot6^7)(4^9\cdot6^3\cdot8^3)_2$ net
5	Mode IV	4,4'-bibp/bridging	86.5(6)/85.6(3)/18.1(8)	3D self-penetrating 4-nodal $(4\cdot5^4\cdot6)_2(4\cdot6^5\cdot7\cdot8^3)_2(5\cdot6\cdot7\cdot8^3)_2(5^2\cdot8^3\cdot9^2)$ net
5	Mode V	4,4'-bibp/bridging	71.0(9)/76.7(2)/11.3(7)	3D self-penetrating 4-nodal $(4\cdot5^4\cdot6)_2(4\cdot6^5\cdot7\cdot8^3)_2(5\cdot6\cdot7\cdot8^3)_2(5^2\cdot8^3\cdot9^2)$ net
6	Mode VI	1,4-bidb/bridging	66.8(7)/82.6(1)/78.9(2)	1D ladder chain

Structural comparisons. As shown in the Scheme 3 and Table 2, the semirigid H_3BCP ligand adopted six different coordination modes and the final obtained complexes display diverse structures. In complex **1**, the H_3BCP is partly deprotonated but coordinated three Co^{II} ions with three η^1:η^0 mode carboxyl groups (Mode I), obtained 1D ladder chains, which are expanded by the bridged 1,4-bib ligands to a 3-fold 2D→2D interpenetrated (3,4)-connected networks. For complex **2**, the H_3BCP is completely deprotonated and adopted (κ^1-κ^1)-(κ^1-κ^0)-(κ^1-κ^0)-μ_4 mode (Mode II) bridged the metal centres to form 2D sheets, which are further extended by the 1,4-bib ligands to generate a 2-fold 3D→3D interpenetrated (4,4,6)-connected porous networks. At the same times, the other 1,4-bib ligands act as guest molecules to fulfil the voids, make the whole structure more stability though weak interactions. In complex **3**, the H_2BCP^- anions act as guest molecules, linked with the 2D $[Ni(1,4\text{-bib})]_n$ nets through hydrogen bonds, finally given a 3D supramolecular. It is noteworthy that in complex **4**, the BCP^{3-} adopted (κ^1-κ^1)-(κ^1-κ^1)-(κ^1-κ^1)-μ_6 mode (Mode III) to connect with six 1D $[Fe_4(COO)_6(HCOO)_2]_n$ chains, successfully obtained a 2D $[Fe(BCP)(HCOO)]_n$ sheet. And then the bridging 4,4'-bibp further expanded to a 3D network. There are two kinds coordination modes in the assembly of complex **5**, one BCP^{3-} linked four Ni^{II} ions in a (κ^1-κ^1)-(κ^1-κ^0)-(κ^1-κ^1)-μ_3 mode (Mode IV), and the other linked two Ni^{II} ions by using η^1:η^0-monodentate and η^1:η^1-cheating carboxyl groups (Mode V). In those coordination modes, 3D self-penetrating (4,4,4,5)-coordinated frameworks were constructed under the bridging 4,4'-bibp and μ_2-H_2O help. In complex **6**, the partly deprotonated $HBCP^{2-}$ serve as charge balance as well as the terminal ligand by using its η^1:η^0-monodentate carboxyl group (Mode VI), constructed 1D ladder chains with the help of bridging 1,4-bidb ligands.

Structural investigation of these title complexes reveals that the H_3BCP based coordination polymers, varied from 1D ladder chain (**6**), 2D sheet (**3**), 2D→2D parallel entangled network (**1**), 3D intriguing (4,6,6)-connected framework (**4**), 3D self-penetrating framework (**5**), to 3D→3D parallel entangled framework (**2**). Systematic comparisons between **2** and **3** revealed the pH value of reaction system plays an important factor on the deprotonation of aromatic carboxylic acids and the formation of final architectures. In additions, structures of **2** and **3** are also controlled by the reaction solvent systems. Complexes **5** and **6** are synthesis under similar conditions except the ancillary imidazole linkers, when the 1,4-bidb was replaced by 4,4'-bibp, the structure turned from the 1D ladder chains based supramolecular to 3D self-penetrating (4,4,4,5)-coordinated $(4\cdot5^4\cdot6)_2(4\cdot6^5\cdot7\cdot8^3)_2(5\cdot6\cdot7\cdot8^3)_2(5^2\cdot8^3\cdot9^2)$ frameworks. Last but not least, different transition metal centres in assembly the coordination polymers also have preferences when coordinated with imdizole linkers, which can proved by the structural

comoparisons of **1**/**2** and **4**/**5**. All in all, the obtained final structures are the result of multiple factors.

Thermal Analyses. The experiments of thermogravimetric analysis (TG) were performed on samples of **1**–**6**, shown in Figure S4. For complex **1**, the whole structure began to collapse at about 300°C with a result of thermal decomposition (obsd. 16.1%, calcd. 14.9%). For complex **2**, the first loss at about 100°C is consistent with the removal of coordinated water molecules (obsd. 7.0%, calcd. 7.3%). The second weight loss in the range of 170-220°C can be attributed to the loss of 1,4-bib guest molecules (obsd. 13.7%, calcd. 14.2%). Then the frameworks begin to collapse at about 410°C. For complex **3**, the weight loss below 105 °C can be attributed to the release of coordinated water (obsd: 3.3%; calcd: 2.8%). With the temperature increasing, the H_2BCP^- guest molecules were lost. And then, the host network begins to collapse. For **4**, the weight loss of water molecules is observed at about 115 °C (obsd: 8.9 % and calcd: 8.3 %). The decomposition of organic ligands began from 350 °C, with a result of thermal decomposition (obsd. 19.1%, calcd. 18.4%). For complex **5**, the release of coordinated water molecules (obsd: 3.9%; calcd: 3.5%) in the temperature range of 85–135 °C took place. The framework can be stable until about 380°C, finally given thermal stability unknown solid powder. For complex **6**, the weight loss from 90 to 135 °C is attributed to the release of water molecules (obsd: 7.9%; calcd: 8.3%). Above 260 °C, it starts to lose its ligands, finally given a result of thermal decomposition (obsd. 9.6%, calcd. 8.8%).

XPS analysis. In order to prove the oxidation state of Mn, Co, and Fe ions in related complexes, the XPS measurements were performed using a VG 220i XL system with 12.5 eV as pass energy and monochromatic Al-*Ka* X-ray excitation.

As can be seen in the Fig. S5, the measured binding energy of 781.62 eV for **1** is consistent with the oxidation state of Co^{II}. For two Mn complexes, the XPS of **2** (Mn2p3: Being energy (BE) = 641.46 eV, Mn2p1: BE =652.07 eV) and **3** (Mn2p3: Being energy (BE) = 640.37 eV, Mn2p1: BE =651.02 eV) is in close with the +2 oxidation state of Mn ions. For complex **4**, the measured Fe2p3 and Fe2p1 binding energy are 708.92 eV, and 723.19 eV, indicadated the oxidation state of Fe ions is +2. It is noteworthy that the Fe(II) based CPs under solvothermal reactions are rarely reported.[16] All the metal ions being energy are in close with the ones in NIST X-ray Photoelectron Spectroscopy Database.[17]

Magnetic Properties. The variable-temperature magnetic susceptibility of **2** and **4** were performed because the $[Mn_3(COO)_6]$ SBUs in complex **2** and the $[Fe_4(COO)_6(HCOO)_2]_n$ chain in complex **4** may be holding good magnetic properties. The above-mentioned complexes were tested in the temperature range of 2-300 K under a field of 1000 Oe.

As can be seen in Fig. 7, the $\chi_M T$ value of **2** at 300 K is 9.87 cm^3 K mol^{-1}, lower than the theoretical value of the spin-only value (13.12 cm^3 K mol^{-1}) of three magnetically isolated Mn^{II} ions. With the temperature decreasing, the $\chi_M T$ value decreases continuously to 9.22 cm^3 K mol^{-1} at 40 K. Then the $\chi_M T$ value increases rapidly up to a maximum value of 9.45 cm^3 K mol^{-1} at 34 K. With the temperature further decreasing, the $\chi_M T$ value drops rapidly to 3.03 cm^3 K mol^{-1} at 2K. The temperature dependence χ_M followed the Curie-Weiss law $\chi_M = C/(T-\theta)$ with C= 9.97 cm^3 K mol^{-1}, θ= –4.11 K (Fig. S6). The negative value of θ indicates the presence of an antiferromagnetic interaction between Mn^{II} ions. The above characteristics clearly suggest overall antiferromagnetic interactions between Mn^{II} ions in compound **2**.[18]

For compound **4**, the $\chi_M T$ value is 11.02 cm^3 K mol^{-1} at 300 K, shown in Fig. 8. The susceptibility curve ($\chi_M T$) decreases monotonically when cooling, reaching the lowest value of 1.82 cm^3 K mol^{-1} at 2K with the molar susceptibility χ_M shows a maximum. The temperature dependence χ_M^{-1}-T is nonlinear, the χ_M^{-1} value at 300 K is 27.54 mol cm^{-3}, and with the temperature decreasing, the $\chi_M T$ value decreases continuously to 2.32 mol cm^{-3} at 0.2 K. The temperature dependence χ_M also clearly indicated very strong antiferromagnetic coupling between Fe^{II} ions in compound **4** (Fig. S7).[19]

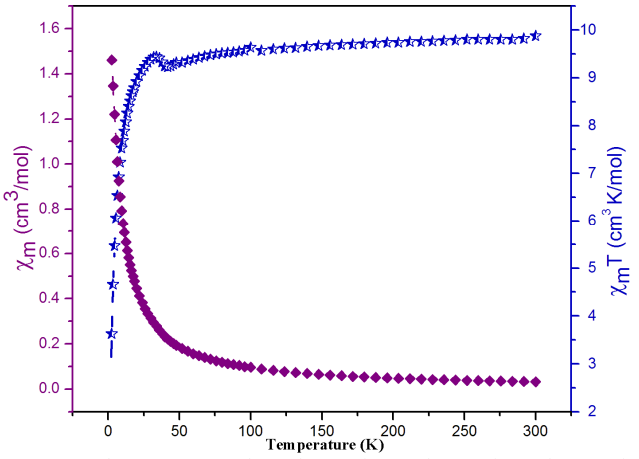

Figure 7. The temperature dependence of χ_M and $\chi_M T$ of **2** under a static field of 1000 Oe.

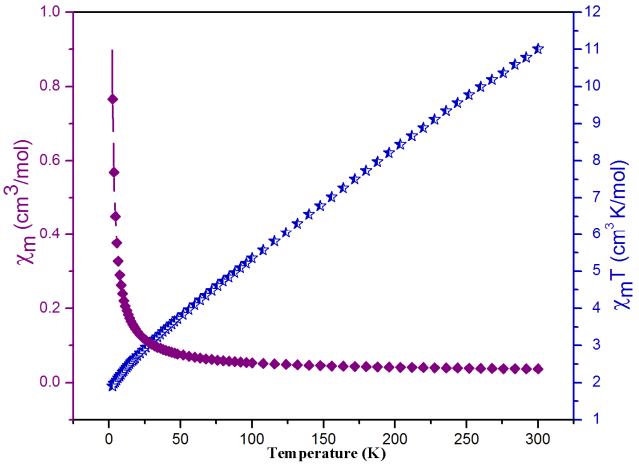

Figure 8. The temperature dependence of χ_M and $\chi_M T$ of **4** under a static field of 1000 Oe.

Conclusions

In summary, we have successfully designed and synthesized six coordination polymers based on 3,5-bi(4-carboxyphenoxy)benzoic acid and three rigid ancillary bridging imidazole linkers. Complexes **1**–**6** displayed appealing structural features varied from 1D ladder chain (**6**),

2D sheet (**3**), 2D→2D parallel entangled network (**1**), 3D intriguing (4,6,6)-connected framework (**4**), 3D self-penetrating framework (**5**), to 3D→3D parallel entangled framework (**2**). Magnetic studies indicate that complexes **2** and **4** both show antiferromagnetic properties.

Acknowledgements

The work was supported by financial support from the Natural Science Foundation of China (Grant Nos. 21101097, 91022034 and 51172127), the Excellent Youth Foundation of Shandong Scientific Committee (Grant JQ201015).

Notes

The authors declare no competing financial interest.

References

1. (a) M. Zhang, W. Lu, J. R. Li, M. Bosch, Y. P. Chen, T. F. Liu, Y. Liu and H. C. Zhou, *Inong. Chem. Front.*, 2014, **1**, 159; (b) J. Duan, M. Higuchi, R. Krishna, T. Kiyonaga, Y. Tsutsumi, Y. Sato, Y. Kubota, M. Takata and S. Kitagawa, *Chem. Sci.*, 2014, **5**, 660; (c) B. L. Chen, N. W. Ockwig, A. R. Millward, D. S. Contreras and O. M. Yaghi, *Angew. Chem. Int. Ed*., 2005, **44**, 4745; (d) J. Duan, Z. Yang, J. Bai, B. Zheng, Y. Li and S. Li, *Chem. Commun*., 2012, **48**, 3058; (e) P. V. Dau and S. M. Cohen, *Chem. Commun.*, 2013, **49**, 6128; (f) W. Y. Zhang, Y. F. Han, L. H. Weng and G. X. Jin, *Organometallics*, **2014**, *33*, 3091.
2. (a) G. Férey and C. Serre, *Chem. Soc. Rev*., 2009, **38**, 1380; (b) H. Fei, J. F. Cahill, K. A. Prather and S. M. Cohen, *Inorg. Chem.*, 2013, **52**, 4011; (c) M. Kim, J. F. Cahill, H. Fei, K. A. Prather and S. M. Cohen, *J. Am. Chem. Soc*., 2012, **134**, 18082; (d) Y. Cui, Y. Yue, G. Qian and B. L. Chen, *Chem. Rev.*, 2012, **112**, 1126.
3. (a) D. Sun, S. Yuan, H. Wang, H. F. Lu, S. Y. Feng and D. F. Sun, *Chem. Commun*., 2013, **49**, 6152; (b) X. T. Zhang, L. M. Fan, X. Zhao, D. Sun, D. C. Li and J. M. Dou, *CrystEngComm*, 2012, **14**, 2053; (c) X. Zhang, L. Fan, W. Zhang, Y. Ding, W. Fan and X. Zhao, *Dalton. Trans*., 2013, **42**, 16562; (d) J. B. Lin, W. Xue, B. Y. Wang, J. Tao, W. X. Zhang, J. P. Zhang and X. M. Chen, *Inorg. Chem*., 2012, **51**, 9423; (e) K. Wang, S. Zeng, H. Wang, J. Dou and J. Jiang, *Inong. Chem. Front.*, 2014, **1**, 167.
4. (a) F. Cao, S. Wang, D. Li, S. Zeng, M. Niu, Y. Song and J. Dou *Inorg. Chem.*, 2013, **52**, 10747; (b) X. T. Zhang, D. Sun, B. Li, L. M. Fan, B. Li and P. H. Wei, *Cryst. Growth Des.*, 2012, **12**, 3845; (c) J. Gao, Y. Gao, Y. Wang, C. Du and Z. Li, *Chem. Commun*., 2013, **49**, 6897; (d) J. Y. Zou, W. Shi, H. L. Gao, J. Z. Cui and P. Cheng, *Inong. Chem. Front.*, 2014, **1**, 242.
5. (a) S. Chen, R. Shang, K. L. Hu, Z. M. Wang and S. Gao, *Inong. Chem. Front.*, 2014, **1**, 83; (b) Y. Wang, H. X. Lin, L. Chen, S. Y. Ding, Z. C. Lei, D. Y. Liu, X. Y. Cao, H. J. Liang, Y. B. Jiang and Z. Q. Tian, *Chem. Soc. Rev*., 2014, **43**, 399; (c) H. Zhou, G. X. Liu, X. F. Wang and Y. Wang, *CrystEngComm.*, 2013, **15**, 1377; (d) S. Y. Song, X. Z. Song, S. N. Zhao, C. Qin, S. Q. Su, M. Zhu, Z. M. Hao and H. J. Zhang, *Dalton. Trans*., 2012, **41**, 10412.
6. (a) L. Li, J. Ma, C. Song, T. Chen, Z. Sun, S. Wang, J. Luo and M. Hong, *Inorg. Chem.*, 2012, **51**, 2438; (b) C. C. Ji, J. Li, Y. Z. Li, Z. J. Guo and H. G. Zheng, *CrystEngComm.,* 2011, **13**, 459; (c) D. Sun, L. L. Han, S. Yuan, Y. K. Deng, M. Z. Xu and D. F. Sun, *Cryst. Growth Des.*, 2013, **13**, 377; (d) X. Zhang, L. Fan, Z. Sun, W. Zhang, W. Fan, L. Sun and X. Zhao, *CrystEngComm*, 2013, **15**, 4910; (e) L. Fan, W. Fan, W. Song, G. Liu, X. Zhang and X. Zhao, *CrystEngComm*, 2014, DOI: 10.1039/C4CE01139B.
7. (a) X. H. Chang, J. H. Qin, M. L. Han, L. F. Ma and L. Y. Han, *CrystEngComm*, 2014, **16**, 870; (b) N. Zhang, Y. Tai, M. Liu, P. Ma, J. Zhao and J. Niu, *Dalton Trans.,* 2014, **43**, 5182; (c) W. Meng, Z. Xu, J. Ding, D. Wu, X. Han, H. Hou and Y. Fan, *Cryst. Growth Des.*, 2014, **14**, 730; (d) L. Fan, X. Zhang, D. Li, D. Sun, W. Zhang and J. Dou, *CrystEngComm*, 2013, **15**, 349; (e) L. Liu, C. Yu, J. Sun, P. Meng, F. Ma, J. Du and L. Ma, *Dalton Trans.,* 20134, **43**, 2915.
8. (a) J. J. Wang, T. T. Wang, L. Tang, X. Y. Hou, M. L. Zhang, L. J. Gao, F. Fu and Y. X. Ren, *Z. Anorg. Allg. Chem.*, 2014, **640**, 483; (b) Y. B. Wang, Y. L. Lei, S. H. Chi and Y. J. Luo, *Dalton Trans.,* 2013, **42**, 1862; (c) Q. Yu, Q. Zhang, H. Bian, H. Liang, B. Zhao, S. Yan and D. Liao, *Cryst. Growth Des.*, 2008, **8**, 1140; (d) X. Zhang, L. Fan, W. Song, W. Fan, L. Sun and X. Zhao, *RSC Adv.*, 2014, **4**, 30274; (e) X. Chang, J. Qin, M. Han, L. Ma and L. Wang, *CrystEngComm*, 2014, **16**, 870.
9. (a) G. L. Liu and H. Liu, *CrystEngComm*, 2013, **15**, 6870; (b) C. Zhan, C. Zou, G. Q. Kong and C. D. Wu, *Cryst. Growth Des.*, 2013, **13**, 1429; (c) J. J. Wang, T. T. Wang, L. Tang, X. Y. Hou, L. J. Gao, F. Fu and M. L. Zhang, *J. Coord. Chem.*, 2013, **66**, 3979; (d) L. Fan, Y. Gao, G. Liu, W. Fan, W. Song, L. Sun, X. Zhao and X. Zhang, *CrystEngComm*, 2014, **16**, 7649; (e) X. Chang, Y. Zhao, M. Han, L. Ma and L. Wang, *CrystEngComm*, 2014, **16**, 6417.
10. (a) Q. L, Zhang, G. W. Feng, Y. Q. Zhang and B. X. Zhu, *RSC Advances*, 2014, **4**, 11384; (b) B. Guo, L. Li, Y. Wang, Y. Zhu and G. Li, *CrystEngComm*, 2013, **42**, 14268; (c) M. L. Han, S. C. Wang and D. F. Feng, *Cryst. Res. Technol.*, 2014, **49**, 276; (d) Q. L. Zhang, P. Hu, Y. Zhao, G. W. Feng, Y. Q. Zhang, B. X. Zhu and Z. Tao, *J. Solid State Chem.*, 2014, **210**, 178.
11. (a) F. Guo, B. Zhu, M. Liu, X. Zhang, J. Zhang and J. Zhao, *CrystEngComm*, 2013, **15**, 6191; (b) L. Fan, X. Zhang, W. Zhang, Y. Ding, W. Fan, L. Sun, Y. Pang and X. Zhao, *Dalton Trans.,* 2014, **43**, 6701; (c) X. Zhang, L. Fan, W. Zhang, W. Fan, L. Sun and X. Zhao, *CrystEngComm*, 2014, **16**, 3203; (d) B. Liu, L. Wei, N. N. Li, W. P. Wu, H. Miao, Y. Y. Wang and Q. Z. Shi, *Cryst. Growth Des*., 2014, **14**, 1110; (e) L. Zhang, J. Guo, Q. Meng, R. Wang and D. Sun, *CrystEngComm*, 2013, **15**, 9578.
12. (a) M. L. Han, X. H. Chang, X. Feng, L. F. Ma and L. Y. Wang, *CrystEngComm*, 2014, **16**, 1687; (b) C. Q. Wang, Y. Zhang, X. Z. Sun and H. J. Yan, *CrystEngComm*, 2014, **16**, 2959; (c) X. L. Wang, Y. Qu, G. C. Liu, J. Luan, H. Y. Lin and X. M. Kan, *Inorg. Chem. Acta*, 2014, **412**, 104; (d) K. K. Bisht, Y. Rachuri, B. Parmar and E. Suresh, *J. Solid State Chem.*, 2014, **213**, 43.
13. (a) L. L. Liu, C. X. Yu, Y. Zhou, J. Sun, P. P. Meng, D. Liu and R. J. Sa, *Inorg. Chem. Commun*, 2014, **40**, 194; (b) X. T. Zhang, L. M. Fan, Z. Sun, W. Zhang, D. C. Li, J. M. Dou and L. Han, *Cryst. Growth Des*., 2013, **13**, 792; (c) L. Fan, X. Zhang, Z. Sun, W. Zhang, Y. Ding, W. Fan, L. Sun, X. Zhao and H. Lei, *Cryst. Growth Des.*, 2013, **13**, 2462; (d) L. Fan, X. Zhang, W. Zhang, Y. Ding, L. Sun, W. Fan and X. Zhao, *CrystEngComm*, 2014, **16**, 2144.
14. (a) G. M. Sheldrick, *SHELXTL*, version 5.1; Bruker Analytical X-ray Instruments Inc.: Madison, WI, 1998. (b) G. M. Sheldrick, *SHELX-97*, PC Version; University of Gottingen: Gottingen, Germany, 1997.
15. (a) V. A. Blatov, A. P. Shevchenko and V. N. Serezhkin, *J. Appl. Crystallogr.*, 2000, **33**, 1193; (b) The network topology was evaluated by the program "TOPOS-4.0", see: http://www.topos.ssu.samara.ru. (c) V. A. Blatov, M. O'Keeffe and D. M. Proserpio, *CrystEngComm*, 2010, **12**, 44.
16. (a) L. Fan, X. Zhang, Z. Sun, W. Zhang, D. Li, P. Wei, B. Li and J. Dou, *J. Coord. Chem.*, 2012, **65**, 4389; (b) G. Lemercier, E. Mulliez, C. Brouca-Cabarrecq, F. Dahan and J. Tuchagues, *Inorg. Chem.*, 2004, **43**, 2105; (c) W. T. Liu, J. Y. Li, Z. P. Ni, X. Bao, Y. C. Ou, J. D. Leng, J. L. Liu and M. L. Tong, *Cryst. Growth Des.*, 2012, **12**, 1482; (d) X. Bao, W. Liu, L. L. Mao, S. D. Jiang, J. L. Liu, Y. C. Chen and M. L. Tong, *Inorg. Chem.*, 2013, **52**, 6233.
17. NIST X-ray Photoelectron Spectroscopy Database, NIST Standard Reference Database 20, Version 4.1, see: http://srdata.nist.gov/xps/.
18. (a) F. Y. Yi and Z. M. Sun, *Cryst. Growth Des.*, 2012, **12**, 5693; (b) M. Ahmad, M. K. Sharma, R. Das, P. Poddar and P. K. Bharadwaj, *Cryst. Growth Des.*, 2012, **12**, 1571; (c) A. Mukherjee, R. Raghunathan, M.K. Saha, M. Nethaji, S. Ramasesha and A.R. Chakravarty, *Chem. Eur. J.*, 2005, **11**, 3087;
19. (a) M. H. Zeng, S. Gao, X. L. Yu and X. M. Chen, *New J. Chem.*, 2003, **27**, 1599; (b) O. Kahn, *Molecular Magnetism*, Wiley-VCH, New York, 1993.

Dalton Trans.

For Table of Contents Use Only

Table of Contents Graphic and Synopsis

Structural Diversity and Magenetic Properties of Six Metal-Organic Polymers Based on Semirigid Tricarboxylate Ligand of 3,5-Bi(4-carboxyphenoxy)benzoic Acid

Liming Fan, Weiliu Fan, Weikuo Song, Liming Sun, Xian Zhao and Xiutang Zhang

Six 3,5-bi(4-carboxyphenoxy)benzoic acid based coordination polymers, varied from 1D ladder chain, 2D sheet, 2D→2D entangled sheet, 3D (4,6,6)-connected framework, 3D self-penetrating framework, to 3D→3D entangled framework, have been obtained in the presence of three imidazole linkers.